

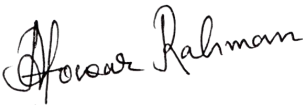
*Dedicate this thesis to my beloved parents
and inspiration*

Abbajan & Ammajan

DECLARATION BY THE CANDIDATE

I hereby declare that the thesis entitled “**Investigations on certain electrode materials for electrochemical capacitors**”, being submitted to **Department of Physics, Tezpur University**, Tezpur, Assam in partial fulfilment for the award of the degree of Doctor of Philosophy in physics and it has not been previously considered for the award of any degree, diploma, associateship, fellowship or any other similar title or recognition from any University, Institute or other organizations.

Date: 23-04-2025


Atowar Rahman

Place: Tezpur

Enrollment No: PHP19107

Registration No: TZ203797 of 2021



TEZPUR UNIVERSITY

(A Central University established by an Act of Parliament)

Napaam, Tezpur-784028

DISTRICT: SONITPUR, ASSAM, INDIA

Dr. Shyamal Kumar Das

Phone: 03712-275586

Assistant Professor

Email: skdas@tezu.ernet.in

Department of Physics

School of Sciences, Tezpur University

CERTIFICATE OF THE SUPERVISOR

This is to certify that the thesis entitled “**Investigations on certain electrode materials for electrochemical capacitors**”, submitted to the school of sciences, Tezpur University in requirement of partial fulfilment for the award of the degree of Doctor of Philosophy in physics is a record of research work carried out by Mr. Atowar Rahman under my supervision and guidance.

All help received by him from various sources have been duly acknowledged.

No part of this thesis has been submitted elsewhere for award of any degree.

Date: 23-04-2025

(Shyamal Kumar Das)

Place: Tezpur

Principal Supervisor

ACKNOWLEDGEMENT

At first, I thank the Almighty for sending me in the Earth, opportunities in my life, blessings me throughout this challenging Ph.D. journey, keeping me safe, happy, and constantly moving forward.

I am deeply honored and filled with immense joy as I express my heartfelt gratitude to my former esteemed supervisor, late Prof. Ashok Kumar, Professor in the Department of Physics at Tezpur University, whose guidance was pivotal in the initial stage of my PhD. His inspirations, constructive discussions and encouragements highly motivated me in the research work.

It is with great pleasure that I extend my profound thanks to my current supervisor, Dr. Shyamal Kumar Das, for his dynamic leadership and meticulous supervision. His unwavering support, encouragement, and insightful guidance were crucial to the success of this work. I am fortunate to have benefitted from his invaluable wisdom and dedicated involvement throughout my doctoral journey. I will forever cherish the mentorship and training he has provided me.

I would also like to express my sincere gratitude to my doctoral committee members, Dr. Rajib Biswas from the department of Physics and Prof. Kusum K. Bania from the Department of Chemistry at Tezpur University, Assam, for their insightful advice and guidance throughout my research.

I am deeply thankful to the former Vice Chancellor, Prof. V. K. Jain, and the current Vice-Chancellor, Prof. Shambhu Nath Singh of Tezpur University, for providing the necessary facilities and academic environment that supported my Ph.D. studies.

I also wish to express my gratitude to Prof. Pabitra Nath, Head of the Department of Physics, for offering essential research resources and his continuous support.

I would like to thank Council of Scientific and Industrial Research (CSIR), New Delhi, for the NET-JRF. I also extend my sincere gratitude to DST-SERB for the AUTOLAB 302N Modular Potentiostat Galvanostat, Netherlands (instrument) where I performed all the important measurements of my thesis.

I would like express my sincere appreciation to SAIC, Tezpur University for providing access to advanced instrumentation for material characterization, NECBH at IITG for facility.

I am grateful to Tezpur University for providing me with this invaluable opportunity. The university's exceptional facilities and work-oriented environment have significantly contributed to my academic and personal growth.

I extend my sincere thanks to all the teachers in the Department of Physics, Tezpur University for their unwavering support and encouragement throughout my research.

I appreciate the help of all the staff members in the Department of Physics. Special thanks to Narayan da and Patir da, for their timely assistance and support.

I would also like to thank the past and present members of the Material Research Laboratory and Energy Storage Laboratory, Department of Physics, Tezpur University, with whom I had the privilege to work. Special mentions include Rituraj Da, Bhagyalakhi, Ba, Devalina Ba, Kashmiri, Ankush, Kakoli, Sushmita, Sunny, Ritupurna and Konica. My gratitude extends to all the research scholars, Department of Physics, for their assistance and insightful discussions.

Words cannot express my gratitude for the unwavering love, support and blessings I have received from my "Abbajan and Ammajan." You both mean the world to me, and I am deeply thankful for everything.


I also owe a debt of gratitude to my sisters (Lotifa and Moriom) for their unconditional love.

A special mention goes to my wife (Dr. Sultana Parven) for being there for me during the highs and lows of my Ph.D. journey.

I would like to thank my in laws for their encouragement and supports during the phase of my Ph.D.

I would like to thank all those who have supported me in various ways but whose names I could not mention here. I am forever grateful to you all.

Date: 23-04-2025


(Atowar Rahman)

LIST OF TABLES

<u>Table No.</u>	<u>Table caption</u>	<u>Page No.</u>
	CHAPTER 1	
Table 1.1	Comparison of abundance, ionic radius and volumetric capacities of some selective metal ions	9
	CHAPTER 2	
Table 2.	Specific capacitance of MoO ₃ //MoO ₃ and rGO/MoO ₃ //rGO/MoO ₃ cells in aqueous and gel electrolytes at different current densities	50
Table 2.2	Comparison of energy and power density of our present work with literature.	53-54
	CHAPTER 3	
Table 3.1	Comparison of the difference of specific capacitance between 5 th and 45 th cycle for the potential windows of (0-1.5) V, (0-1.7) V and (0-2) V at current density of 0.5 Ag ⁻¹	73
	CHAPTER 4	
Table 4.1	Comparison of stable specific capacitances at different electrolytes	94
Table 4.2	Specific capacitance of VA // VA cells at different Current densities in aqueous and gel electrolytes	98

LIST OF FIGURES

<u>Figure No.</u>	<u>Figure caption</u>	<u>Page No.</u>
CHAPTER 1		
Figure 1.1	Ragone plot of different electrochemical devices	2
Figure 1.2	Block diagram of different classes of supercapacitors	5
Figure 1.3	Mechanism of EDLC type electrochemical capacitors (supercapacitors)	6
Figure 1.4	Three different pseudocapacitors: (a) Intrinsic pseudocapacitor, (b) Intercalation pseudocapacitor and (c) Extrinsic pseudocapacitor	8
CHAPTER 2		
Figure 2.1	Schematic diagram of electrospinning setup	36
Figure 2.2	Digital photographs of (a) 1 M AlCl ₃ aqueous electrolyte and (b) 1 M AlCl ₃ -PVA gel electrolyte	38
Figure 2.3	XRD patterns of PVA/ammonium molybdate composite nanofibers, MoO ₃ and rGO/MoO ₃ nanorods	39
Figure 2.4	(a) Thermogravimetric analysis (TGA) curve of PVA/ammonium molybdate composite nanofibers and rGO/PVA/ammonium molybdate composite nanofibers and (b) XRD patterns of graphene oxide (GO) and reduced graphene oxide (rGO)	39
Figure 2.5	Raman spectra of MoO ₃ and rGO/MoO ₃ nanorods with inset views in the range of 1500 cm ⁻¹ to 1800 cm ⁻¹ to show the G band	40
Figure 2.6	SEM images of (a) PVA/ammonium molybdate composite nanofibers, (b) MoO ₃ nanorod after calcination, (c) rGO/PVA/ammonium molybdate composite nanofibers and (d) rGO/MoO ₃ nanorod after calcination	40
Figure 2.7	CV curves of (a) MoO ₃ nanorod and (b) rGO/MoO ₃ nanorod in 1 M AlCl ₃ aqueous electrolyte, (c) rGO/MoO ₃ in gel electrolyte (1 M AlCl ₃ -PVA)	42
Figure 2.8	CV curves of MoO ₃ //MoO ₃ symmetric cell in 1 M AlCl ₃	43

	aqueous electrolyte in the potential window of (a) (0-1.3) V and (b) (0-1.5) V, (c) (0-1.7) V and (d) (0-1.9) V	
Figure 2.9	CV curves of MoO ₃ //MoO ₃ and rGO/MoO ₃ //rGO/MoO ₃ in the potential range of (0-1.5) V at scan rates of (a) 2 mVs ⁻¹ , (b) 3 mVs ⁻¹ , (c) 100 mVs ⁻¹ in 1 M AlCl ₃ aqueous electrolyte	43
Figure 2.10	CV curves of rGO/MoO ₃ //rGO/MoO ₃ symmetric cell in gel electrolyte (1 M AlCl ₃ -PVA) in the potential window of (a) (0-1.5) V, (b) (0-2) V, (c) (0-2.2) V and (d) (0-2.4) V. The scan rate is 2 mVs ⁻¹	44
Figure 2.11	CV curves of MoO ₃ //MoO ₃ cell in the potential range of (0-1.5) V at scan rate of (a) 3 mVs ⁻¹ , (b) 5 mVs ⁻¹ , (c) 7 mVs ⁻¹ , 10 mVs ⁻¹ , (e) 50 mVs ⁻¹ , and (f) 100 mVs ⁻¹ in aqueous electrolyte (1 M AlCl ₃)	45
Figure 2.12	CV curves of rGO/MoO ₃ //rGO/MoO ₃ cell in the potential range of (0-1.5) V at scan rate of (a) 3 mVs ⁻¹ , (b) 5 mVs ⁻¹ , (c) 7 mVs ⁻¹ , (d) 10 mVs ⁻¹ , (e) 50 mVs ⁻¹ , and (f) 100 mVs ⁻¹ in aqueous electrolyte (1 M AlCl ₃)	45
Figure 2.13	CV curves of rGO/MoO ₃ //rGO/MoO ₃ cell in the potential range of (0-2) V at scan rate of (a) 3 mVs ⁻¹ , (b) 5 mVs ⁻¹ , (c) 7 mVs ⁻¹ , (d) 10 mVs ⁻¹ , (e) 50 mVs ⁻¹ and (f) 100 mVs ⁻¹ in gel electrolyte (1 M AlCl ₃ -PVA)	46
Figure 2.14	Electrolyte stability test. CV curves obtained from a Ti-Ti cell in 1 M AlCl ₃ aqueous electrolyte at scan rate of 2 mVs ⁻¹ in the voltage range of (a) (0-1.3) V, (b) (0-1.5) V, (c) (0-1.7) V, (d) (0-2.2) V. (e) comparison of all the CV profiles	47
Figure 2.15	Electrolyte stability test. CV curves of (a) Ti-Ti cell and MoO ₃ //MoO ₃ cell in 1 M AlCl ₃ aqueous electrolyte at scan rate of 2 mVs ⁻¹ , the magnified version of (a) is shown in (b). CV curves of (c) Ti-Ti cell and rGO/MoO ₃ //rGO/MoO ₃ cell in gel electrolyte (1 M AlCl ₃ -PVA), the magnified version of (c) is shown in (d).	48
Figure 2.16	Electrolyte stability test. CV curves obtained from a Ti-Ti cell in gel electrolyte (1 M AlCl ₃ -PVA) at scan rate of 2 mVs ⁻¹ in the voltage range of (a) (0-2) V and (b) (0-2.4) V. (c)	49

	comparison of all the CV profiles	
Figure 2.17	Galvanostatic charge/discharge curves of (a) $\text{MoO}_3//\text{MoO}_3$ cell in 1 M AlCl_3 aqueous electrolyte, (b) $\text{rGO}/\text{MoO}_3//\text{rGO}/\text{MoO}_3$ cell in 1 M AlCl_3 aqueous electrolyte and (c) $\text{rGO}/\text{MoO}_3//\text{rGO}/\text{MoO}_3$ in gel electrolyte (1 M AlCl_3 -PVA)	50
Figure 2.18	Rate performances of $\text{MoO}_3//\text{MoO}_3$ and $\text{rGO}/\text{MoO}_3//\text{rGO}/\text{MoO}_3$ cells in aqueous and gel electrolyte	52
Figure 2.19	(a) Long-term cycle performance at current density of 1 Ag^{-1} up to 1000 cycles and (b) plot of energy density vs power density at different current densities	52
Figure 2.20	self-discharge curves in aqueous and gel electrolytes	54
CHAPTER 3		
Figure 3.1	Schematic diagram of synthesis of polyaniline	61
Figure 3.2	Schematic diagram of synthesis of vanadium oxy-acetylacetonate	61
Figure 3.3	XRD pattern and FESEM image of (a, b) VOA and (c, d) PANI Respectively	63
Figure 3.4	(a) Raman and (b) FTIR spectra of PANI	63
Figure 3.5	CV profiles of VOA in (a) 1 M AlCl_3 , (b) 0.5 M $\text{Al}_2(\text{SO}_4)_3$ and (c) 1 M $\text{Al}(\text{NO}_3)_3$ aqueous electrolytes	
Figure 3.6	Discharge-charge profile of (a) VOA and (b) capacity versus cycle number of VOA in 1 M AlCl_3 aqueous electrolyte	65
Figure 3.7	(a) CV profiles (b) Discharge-charge profile and (a) Capacity versus cycle number of PANI in 1 M AlCl_3 aqueous electrolyte	65
Figure 3.8	CV profiles of PANI for the aqueous electrolytes (a) 0.5 M $\text{Al}_2(\text{SO}_4)_3$ and (b) 1 M $\text{Al}(\text{NO}_3)_3$, Charge-discharge profiles of PANI for the aqueous electrolytes (c) 0.5 M $\text{Al}_2(\text{SO}_4)_3$ and (d) 1 M $\text{Al}(\text{NO}_3)_3$ and (e) Comparison of long cycling stability of PANI for all the aqueous electrolytes	66
Figure 3.9	CV profiles of (a) PANI and (c) VOA at different scan rates. Plot of log (peak current) vs log (scan rate) for (b) PANI and (d) VOA	67
Figure 3.10	CV profiles of VOA in 1 M AlCl_3 aqueous electrolyte at different scan rates. [NOTE: it was difficult to identify the cathodic peak in the	68

case of VOA at higher scan rates. Therefore, to calculate the b value, the most distinct anodic peak (labeled as peak C) is considered.]

Figure 3.11	CV profiles of PANI in 1 M AlCl_3 aqueous electrolyte at different scan rates	68
Figure 3.12	CV profiles of VOA in (a) 1 M HCl and (b) 0.5 M H_2SO_4 , CV profiles of PANI in (c) 1 M HCl and (d) 0.5 M H_2SO_4	69
Figure 3.13	Schematic diagram of VOA/PANI cell	70
Figure 3.14	CV profiles of VOA/PANI asymmetric supercapacitor in different potential windows	70
Figure 3.15	Charge-discharge profiles of VOA/PANI in the potential windows of (a) (0-1.5) V, (b) (0-1.7) V, (c) (0-2) V at current density of 0.5 Ag^{-1}	71
Figure 3.16	Rate capability of VOA/PANI in the potential windows of (a) (0-1.5) V, (b) (0-1.7) V, (c) (0-2) V	71
Figure 3.17	(a) Energy density vs power density plot and (b) Long term stability curve in the potential window (0-2) V	72
Figure 3.18	Snapshot of the demonstration of the VOA/PANI cell to light up a LED light	73
CHAPTER 4		
Figure 4.1	Schematic diagram of synthesis of vanadyl acetate	76
Figure 4.2	Digital photographs of (a) 0.5 M Na_2SO_4 /Gum (gel) and (b) 0.5 M Na_2SO_4 /Silica (gel) electrolytes	78
Figure 4.3	(a) XRD pattern, (b) Raman spectrum, (c) TGA and (d) FESEM image of VA	79
Figure 4.4	CV profiles of VA in (a) 0.5 M $\text{Al}_2(\text{SO}_4)_3$ and (b) 1 M AlCl_3 at a scan rate of 2 mVs^{-1}	79
Figure 4.5	CV profiles of VA in (a) 1 M NaCl and (b) 1 M LiCl aqueous electrolytes	80
Figure 4.6	CV profiles of VA in (a) 1 M HCl and (b) 1 M H_2SO_4 aqueous electrolytes and (c) DI water	80
Figure 4.7	Discharge- charge profiles of VA in (a) 0.5 M $\text{Al}_2(\text{SO}_4)_3$ and (a) 1 M AlCl_3 aqueous electrolytes	81
Figure 4.8	Comparison of long cycle stability of VA in 0.5 M $\text{Al}_2(\text{SO}_4)_3$	82

	and 1 M AlCl ₃ aqueous electrolytes at current density of 1 Ag ⁻¹	
Figure 4.9	CV profiles of VA (a) 1 M AlCl ₃ /NH ₄ OH (aq, pH=3.6) and (b) 1 M AlCl ₃ /NH ₄ OH/PVA (gel, pH=3.4) electrolytes, Discharge-charge profiles of VA in (c) 1 M AlCl ₃ /NH ₄ OH (aq, pH=3.6) and (d) 1 M AlCl ₃ /NH ₄ OH/PVA (gel, pH=3.4) electrolytes and (e) Comparison of cycle stabilities	83
Figure 4.10	(a) XRD and (b) Raman spectrum of VA, rGO/VA and CNT/VA	84
Figure 4.11	FESEM images of (a) rGO, (b) CNT, (c) rGO/VA and (d) CNT/VA	85
Figure 4.12	CV profiles of (a) rGO/VA and (b) CNT/VA at scan rate of 2 mVs ⁻¹ in 1 M AlCl ₃ , charge- discharge profiles of (c) rGO/VA and (d) CNT/VA, (e) Comparison of cycle stability at current density of 1 Ag ⁻¹ in 1 M AlCl ₃ aqueous electrolyte	86
Figure 4.13	Ex-situ XRD of pristine VA electrode and after first charge and first discharge states	87
Figure 4.14	Ex-situ FESEM of (a) pristine VA electrode and (b) after first charge state	87
Figure 4.15	Ex-situ Raman of (a) pristine VA electrode and after 1 st & 20 th discharge states, enlarged view corresponding to (b) yellow, (c) pink and (d) green portions	88
Figure 4.16	CV profiles of (a) VA in 1 M MgSO ₄ and (b) 1 M MgCl ₂ electrolytes at scan rate of 2 mVs ⁻¹ , Charge-discharge profiles of VA in (c) in 1 M MgSO ₄ and (d) 1 M MgCl ₂ electrolytes at current density of 1 Ag ⁻¹ and (e) Comparison of cycle stability at current density of 1 Ag ⁻¹ over 100 cycles	89
Figure 4.17	CV profiles of (a) VA in 0.5 M Na ₂ SO ₄ and (b) 1 M NaCl electrolytes at scan rate of 2 mVs ⁻¹ , Charge -discharge profiles of VA in (c) in 0.5 M Na ₂ SO ₄ and (d) 1 M NaCl electrolytes at current density of 1 Ag ⁻¹ and (e) Comparison of cycle stability at current density of 1 Ag ⁻¹ over 100 cycles	90
Figure 4.18	EDS spectra of VA after 1 st discharge state and the corresponding atomic percentages of the elements (inset table)	91
Figure 4.19	Elemental mappings of VA electrode material after 1 st discharge	91

	state	
Figure 4.20	(a) Ex-situ Raman spectra of VA after 1 st and 20 th discharge states, (b-c) enlarged view of the peaks at 161 cm ⁻¹ , 263 cm ⁻¹ , 510 cm ⁻¹ and 695 cm ⁻¹	92
Figure 4.21	(a) Ex-situ XRD patterns of pristine VA, 1 st discharged and 1 st charged state electrodes, FESEM images of (b) pristine VA electrode, (c) 1 st discharged state and (d) 1 st charged state electrodes in 0.5 M Na ₂ SO ₄ electrolyte	93
Figure 4.22	Comparison of cycling stability at current density of 1 Ag ⁻¹ over 100 cycles in (a) 0.5 M Al ₂ (SO ₄) ₃ , 1 M MgSO ₄ , 0.5 M Na ₂ SO ₄ and (b) 1 M AlCl ₃ , 1 M MgCl ₂ , 1 M NaCl electrolytes over 100 cycles	93
Figure 4.23	Digital Photographs of electrolytes (a) 0.5 M Al ₂ (SO ₄) ₃ , (b) 1 M MgSO ₄ and (c) 0.5 M Na ₂ SO ₄ after 100 cycles	94
Figure 4.24	CV curves of VA // VA symmetric supercapacitor at scan rate of 2 mVs ⁻¹ in 0.5 M Na ₂ SO ₄ (aq) electrolyte for the potential window (a) (0-1.4) V, (b) (0-1.6) V, (c) (0-1.8) V, (d) (0-2) V and (e) (0-2.2) V	95
Figure 4.25	CV profile of Bare graphite // Bare graphite cell in 0.5 M Na ₂ SO ₄ (aq) electrolyte	95
Figure 4.26	CV profiles of VA // VA cell in the potential window (a) (0-1.6) V, (b) (0-1.8) V, (c) (0-2) V, (d) (0-2.2) V in 0.5 M Na ₂ SO ₄ /Gum (gel) electrolyte	96
Figure 4.27	CV profiles of VA // VA cell in the potential window (a) (0-1.6) V, (b) (0-1.8) V, (c) (0-2) V, (d) (0-2.2) V in 0.5 M Na ₂ SO ₄ /Silica (gel) electrolyte	96
Figure 4.28	GDC profiles of VA // VA symmetric supercapacitor at current density of 0.1 Ag ⁻¹ in (a) 0.5 M Na ₂ SO ₄ (aq), (b) 0.5 M Na ₂ SO ₄ /Gum (gel) and (c) 0.5 M Na ₂ SO ₄ /Silica (gel) electrolytes	97
Figure 4.29	Rate capabilities of VA // VA symmetric supercapacitor in aqueous and gel electrolytes	98
Figure 4.30	Comparisons of (a) energy densities vs power densities and (b) long term cycling stabilities (at higher current density 2 Ag ⁻¹ up to 2000 cycles) of VA // VA symmetric supercapacitor	99

in aqueous as well as gel electrolytes

CHAPTER 5

Figure 5.1	(a) XRD pattern, (b) Raman -spectrum and (c) FTIR spectrum of VOH	104
Figure 5.2	(a-b) FESEM images of VOH	105
Figure 5.3	CV profiles of VOH in (a) 0.25 M AlCl_3 , (b) 0.5 M AlCl_3 and (c) 1 M AlCl_3 aqueous electrolytes and (d) the comparison of area under the curves	106
Figure 5.4	CV profiles of VOH in (a) 0.5 M $\text{Al}_2(\text{SO}_4)_3$ and (b) 1 M $\text{Al}(\text{NO}_3)_3$ aqueous electrolytes	107
Figure 5.5	CV profile of VOH in 1 M AlCl_3/PEO (gel) electrolyte	107
Figure 5.6	CV profiles of VOH in (a) 1 M LiCl and (b) 1 M NaCl aqueous electrolytes	108
Figure 5.7	CV profiles of VOH in (a) 1 M HCl and (b) 0.5 M H_2SO_4 aqueous electrolytes	108
Figure 5.8	GCD profiles of VOH in (a) 0.25 M AlCl_3 (b) 0.5 M AlCl_3 , (c) 1 M AlCl_3 aqueous electrolytes and (d) 1 M AlCl_3/PEO (gel) electrolytes	109
Figure 5.9	Specific capacitance versus cycle number at current density of 1 Ag^{-1} over 100 cycles for all the aqueous and gel electrolytes	110
Figure 5.10	Nyquist plots of VOH electrode in 1 M AlCl_3 aqueous and 1 M AlCl_3/PEO gel electrolytes with the equivalent circuit diagram	110
Figure 5.11	GCD profiles of VOH in (a) 0.5 M AlCl_3 , (b) 1 M $\text{Al}(\text{NO}_3)_3$ at current density of 1 Ag^{-1} and (c) Specific capacitance versus cycle number	111
Figure 5.12	(a) CV profiles of VOH at scan rate from 3 mVs^{-1} to 10 mVs^{-1} in 1 M AlCl_3 aqueous electrolyte, (b) log (scan rate) vs log (peak current) plot and (c) charge storage contribution plot	112
Figure 5.13	(a) XRD pattern, (b) Raman and (c) FTIR of AlVOH	113
Figure 5.14	(a-b) FESEM images of AlVOH	113

Figure 5.15	CV profiles of AlVOH in (a) 1 M AlCl ₃ , (b) 0.5 M Al ₂ (SO ₄) ₃ and (c) 1 M Al(NO ₃) ₃ aqueous electrolytes	114
Figure 5.16	GCD profiles of AlVOH in (a) 1 M AlCl ₃ , (b) 0.5 M Al ₂ (SO ₄) ₃ and (c) 1 M Al(NO ₃) ₃ aqueous electrolytes	115
Figure 5.17	Comparison of cycling stability up to 100 cycles at current density of 1 Ag ⁻¹	115
Figure 5.18	(a) CV profiles and (b) GCD profiles of AlVOH in 1 M AlCl ₃ /PEO gel electrolyte and (c) the comparison of cycling stability up to 100 cycles	116

ABBREVIATIONS

<u>Abbreviations/Symbols</u>	<u>Name</u>
MoO ₃	Molybdenum trioxide
GO	Graphene oxide
rGO	Reduced graphene oxide
CNT	Carbon nanotube
PVA	Polyvinyl alcohol
XRD	X-ray diffraction
TGA	Thermogravimetric analysis
FESEM	Field Emission Scanning Electron Microscope
SEM	Scanning Electron Microscope
FTIR	Fourier-transform infrared spectroscopy
NMP	N-Methyl-2-pyrrolidone
PVDF	Polyvinylidene fluoride
EDLC	Electric double layer capacitor
Fg ⁻¹	Farrad per gram
Ag ⁻¹	Ampere per gram
mVs ⁻¹	Millivolt per second
CV	Cyclic voltammetry
GCD	Galvanostatic charge discharge
Al ³⁺ ion	Aluminium ion
mL	Milliliter
g	Gram
mg	Milligram
M	Molar
%	Percent
h	hour
mA	Mili ampere
A	Ampere
s	Second
V	Volt
cm ⁻¹	Per centimeter

°C	Degree Celsius
JCPDS	Joint Committee on Powder Diffraction Standards
AlCl ₃	Aluminium chloride
Al ₂ (SO ₄) ₃	Aluminium sulfate
Al(NO ₃) ₃	Aluminium nitrate
Wh	Watt-hour
kg	Kilogram
W	Watt
wt	Weight
Na ⁺	Sodium ion
Mg ²⁺	Magnesium ion
PANI	Polyaniline
VOA	Vanadium oxy-acetylacetonate
VA	Vanadyl acetate
VOH	Hydrated vanadate
Al	Aluminium
EIS	Electrochemical impedance spectroscopy
MHz	Megahertz
Hz	Hertz
w.r.t	With respect to
MgCl ₂	Magnesium chloride
MgSO ₄	Magnesium sulfate
NaCl	Sodium chloride
Na ₂ SO ₄	Sodium sulfate